Author Manuscript

Author Manuscript

Author Manuscript

Author Manuscript

HHS Public Access

Author manuscript

J Chem Inf Model. Author manuscript; available in PMC 2019 April 10.

Published in final edited form as:

J Chem Inf Model. 2019 January 28; 59(1): 373–385. doi:10.1021/acs.jcim.8b00583.

Mechanism of Hormone Peptide Activation of a GPCR: Angiotensin II Activated State of AT_1R Initiated by van der Waals Attraction

Khuraijam Dhanachandra Singh, **Hamiyet Unal**, **Russell Desnoyer**, and **Sadashiva S. Karnik***

Department of Molecular Cardiology, Lerner Research Institute, Cleveland Clinic Foundation, Cleveland, Ohio 44195, United States

Abstract

We present a succession of structural changes involved in hormone peptide activation of a prototypical GPCR. Microsecond molecular dynamics simulation generated conformational ensembles reveal propagation of structural changes through key “microswitches” within human AT_1R bound to native hormone. The endocrine octa-peptide angiotensin II (AngII) activates AT_1R signaling in our bodies which maintains physiological blood pressure, electrolyte balance, and cardiovascular homeostasis. Excessive AT_1R activation is associated with pathogenesis of hypertension and cardiovascular diseases which are treated by sartan drugs. The mechanism of AT_1R inhibition by sartans has been elucidated by 2.8 Å X-ray structures, mutagenesis, and computational analyses. Yet, the mechanism of AT_1R activation by AngII is unclear. The current study delineates an activation scheme initiated by AngII binding. A van der Waals “grasp” interaction between $Phe8^{AngII}$ with $Ile288^{7.39}$ in AT_1R induced mechanical strain pulling $Tyr292^{7.43}$ and breakage of critical interhelical H-bonds, first between $Tyr292^{7.43}$ and $Val108^{3.32}$ and second between $Asn111^{3.35}$ and $Asn295^{7.46}$. Subsequently changes are observed in conserved microswitches DRY^{TM3}, $Yx7K(R)^{TM5}$, $CWxP^{TM6}$, and $NPxxY^{TM7}$ in AT_1R. Activating the microswitches in the intracellular region of AT_1R may trigger formation of the G-protein binding pocket as well as exposure of helix-8 to cytoplasm. Thus, the active-like conformation of AT_1R is initiated by the van der Waals interaction of $Phe8^{AngII}$ with $Ile288^{7.39}$, followed by systematic reorganization of critical interhelical H-bonds and activation of microswitches.

Graphical Abstract

***Corresponding Author** Mailing address: Lerner Research Institute, Cleveland Clinic, 9500 Euclid Avenue, Cleveland, Ohio 44195, United States of America. karniks@ccf.org.

Notes

The authors declare no competing financial interest.

Author Manuscript Author Manuscript Author Manuscript Author Manuscript

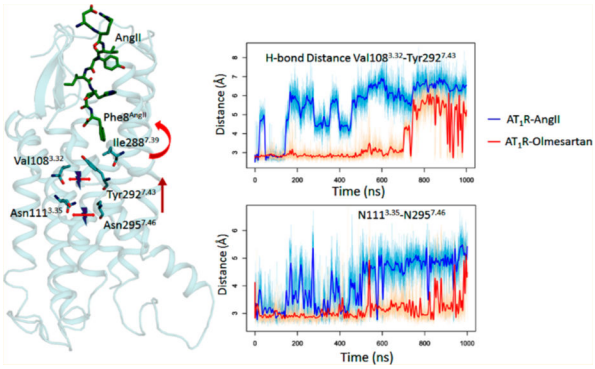

INTRODUCTION

Nearly 5% of the human genome encodes G-protein coupled receptors (GPCRs), which are targets of ~34% of therapeutic drugs currently in use.[1] GPCRs are seven-transmembrane helical proteins that modulate vital cell-signaling responses to a variety of natural and pharmaceutical ligands.[1–5] Extracellular agonists bind and initiate receptor conformational changes which propagate across the trans-membrane (TM) α-helical domain to intracellular "microswitches" formed by highly conserved sequence motifs in GPCRs. These events result in the transient formation of a cytosolic cleft for binding and activating a cognate G protein. By comparing the antagonist-bound inactive and [agonist + G protein/antibody] bound active state structures of GPCRs, the activating structural changes were identified.[6–11] Structure−function studies have shown that mutating a microswitch may still allow the activating motion of TM-helices but impair cell signaling.[12] Intramolecular events that form the electromechanical basis of signal transduction are predominantly documented for amine activated GPCR prototypes. Although three agonist-peptide bound GPCR structures are available (PDB ids: 6DDF, 5UNF, 5T04), an ensemble view of the conformational dynamics of peptide hormone activation of a GPCR is absent to date.[13–16]

The angiotensin type 1 receptor (AT_1R) is a clinically important GPCR that binds the renin −angiotensin system hormone angiotensin II (AngII). Cell signaling by activated AT_1R involves stimulation of the $Gq_{11/12}$ leading to intra-cellular production of calcium, lipid messengers, and activation of protein kinases.[17–20] In addition, G protein-independent signaling pathways are also activated.[21–25] AngII-activated AT_1R is responsible for homeostatic regulation of blood pressure and water−electrolyte balance in the body.[26,27] AT_1R is widely expressed in vascular and myocardial tissue, the liver, the kidney, the adrenal cortex, and specific brain centers. Chronic AT_1R activation produces disease states including hypertension, inflammation, endothelial dysfunction, athero-sclerosis, congestive heart failure, and end organ damage. AT_1R blocking drugs (ARBs) such as olmesartan are used as a first line of therapy in fighting these diseases. Previous studies have suggested a transition scheme for functional states of AT_1R [Figure 1A] upon antagonist and agonist binding.[28,29] Two high-resolution inactive state structures of AT_1R are reported but attempts made to crystallize the AngII bound AT_1R did not succeed.[13,14] To bridge the knowledge gap with regard to the AngII-activated state of AT_1R, we performed microsecond molecular dynamics simulation (MDS) analysis in a membrane bilayer environment.

Author Manuscript Author Manuscript Author Manuscript Author Manuscript

In this first report delineating conformational ensemble of a clinically relevant peptide hormone—GPCR—we carried out MDS starting with the 2.8 Å X-ray crystallographic structure of human AT_1R.[13,14] We corroborate the MDS results [Figure 1B] by (i) comparing to active-state structures of established GPCRs;[30–34] (ii) using stereochemical features of AngII-analogs defined by structure activity relationship (SAR),[35–38] and (iii) by combining with site-directed mutagenesis findings on pharmacology of AT_1R.[37,39–49] As in all GPCRs, several conserved residues form functional motifs within AT_1R [Figure 1C]. During AT_1R-AngII signaling, these motifs may act as microswitches that change from an inactive to an active conformation. Hence, inspecting perturbation in $CWxP^{TM6}$, DRY^{TM3}, $Yx7K(R)^{TM5}$, and $NPxxY^{TM7}$ motifs in comparison to different established activated GPCRs[39–42] will further validate our MDS. SAR analysis of the AngII peptide, Asp^1-Arg^2-Val^3-Tyr^4-Ile^5-His^6-Pro^7-Phe^8 has established that the charged property of Asp^1, Arg^2, Phe^8-COO^- and bulk-hydrophobicity of Tyr^4 determine binding affinity and specificity for AT_1R [Figure S1A]. The aromatic Phe^8 side chain and cumulative influence of Tyr4, His6, and Pro7 are responsible for agonist potency of AngII in AT_1R activation.[50–52] Mutagenesis analysis showed that AngII binding requires residues, $Tyr35^{1.39}$, $Trp84^{2.60}$, $Arg162^{ECL2}$, $Lys199^{5.42}$, and $Asp281^{7.32}$ [Figure S1B]. In addition, the critical role of $Asp74^{2.50}$, $Asn111^{3.35}$, $Arg126^{3.50}$, $Trp253^{6.48}$, $His256^{6.51}$, $Ile288^{7.39}$, $Tyr292^{7.43}$, and $Asn295^{7.46}$ in receptor activation are documented.[37,44,46,48,49,53,54] How these features of the receptor and the hormone cooperatively produce an AngII-activated state of AT_1R is unknown.

Our working hypothesis assumes that microswitches constrain spontaneous activation in the basal state of AT_1R. Distinct interactions of AngII with the AT_1R binding pocket break the prime constraint instigating the microswitches to change from inactive to active conformation in the course of receptor activation. Understanding the details of AngII activation of AT_1R could further help in designing more potent ARBs to prevent AngII associated pathogenesis.

RESULTS

Global Conformational Changes.

In the 1 μS MDS following flexible docking of AngII to membrane embedded AT_1R (PDB id: 4ZUD),[13] the trajectory plot for AngII and the receptor backbone reached equilibrium (Figure S2A). Significant changes in root-mean-square fluctuation (RMSF) was observed in DRY, ECL2, and ICL3 motifs as shown in Figure S2B in the AT_1R-AngII compared to AT_1R-Olmesartan. High fluctuation in these motif may correlate with the activation of the receptor. The RMSD plot indicated significant movement in TM-helices, ECL2, ICL3, and helix-8 (Figure S3). The AT_1R conformation ensembles produced from MDS closely match the crystal structure of peptide-agonist bound ET_BR (PDB id: 5GLH)[16] (Figure 2A and B). The volume of the AngII bound pocket of AT_1R is ~1203.11 ± 335.83 $Å^3$, comparable to the pocket of ET_BR which has a volume of 895.92 $Å^3$ (PDB id: 5GLH).[16] The extracellular portions of TM1, TM3, TM4, TM5, and TM7 move in the AngII-bound state (Figure S4). These structural changes are associated with the orthosteric pocket adopting a compact "closed" configuration enabling strong interactions with AngII. Together the N-terminal tail (NT) and EC-loops (ECL) including the β-strands of ECL2 form a lid-like architecture that

Author Manuscript Author Manuscript Author Manuscript Author Manuscript

covers the orthosteric pocket (Figure 2C and D). Mutagenesis and accessibility mapping studies have predicted ligand-specific movements in NT and ECL regions of AT_1R, especially in the ECL2.[55–57] The water accessible entrance in the apo-AT_1R might facilitate the entry of ligands to the orthosteric pocket.

By contrast, in the intracellular region, the TM1, TM3, TM5, TM6, and TM7 move outward (Figure S4). The movement of ICL3 associated with TM3, TM6, and TM7 opens a crevice that is supposed to bind the G protein (Figure 2C and E), but the opening is not complete as seen in the G_s protein bound β_2AR structure.[40] The outward movement of TM6 is comparatively less than observed in the active state crystal structures of GPCRs.[40] Functional studies in AT_1R have indicated that exposure of the DRY^{TM3} motif, the membrane proximal segments of ICL3, and the $NPxxY^{TM7}$ motif are necessary and sufficient to recruit the G protein.[20] A well-defined helix-8 observed in the inactive state AT_1R shows ~15 Å shift toward the cytoplasmic space with decreased helical stability in a small number of the ensemble frames (Figure S4). Observed conformational change in helix-8 is relevant because functional studies have shown that helix-8 of AT_1R is a hotspot for recruitment of non-G protein signaling molecules such as Jak2, Cam kinase, and Filamin A.[20,58] These AngII-induced receptor conformational changes are not observed when olmesartan is used as the ligand for MDS and the ensemble frames are indicative of agonist bound structures of β_2AR, ET_BR, NT1R, and μ-opioid receptor in which structural changes linking the orthosteric pocket and the cytoplasmic G-protein binding pocket is observed.

AngII Binding Interactions.

Supporting the mutagenesis findings, AngII residues 3−8 are embed within the orthosteric pocket (Figure 3A). $Asp1^{AngII}$ and $Arg2^{AngII}$ extend to the NT and ECL2 and ECL3.[55,56,59–61] Binding of AngII involves ~17 AT_1R residues forming ionic, H-bond, van der Waals, and $\pi-\pi$ stacking interactions (Figure 3B). The conformation of bound AngII observed in our MDS is similar to NMR,[62] flexible docking,[38] or modeling studies.[35] Superimposition of AngII and Olmesartan indicates overlap of their aromatic−acidic pharmacophore groups surrounded by shared residues, $Tyr35^{3.91}$, $Trp84^{2.60}$, $Tyr87^{2.63}$, $Lys199^{5.42}$, $Arg167^{ECL2}$, $Ile288^{7.39}$, and $Tyr292^{7.43}$ which validate competitive antagonism of AngII and ARBs (Figure S5). Mutagenesis studies indicate that these are critical residues for binding both AngII and ARBs (see Table S1).

The octapeptide is oriented so that the $Phe8^{AngII}$ α-carboxyl interaction with $Lys199^{5.42}$ is robust (Figure 3). MDS trajectory analysis of $Phe8^{AngII}$ α-carboxyl H-bond and ionic interaction with $Lys199^{5.42}$ estimated to be >75% in multiple trials. It is known that the $Phe8^{AngII}$ α-carboxyl, if blocked by methylation or amination causes tachphylaxis *in vivo*. $Lys199^{5.42}$ mutation to Ala/Gln in AT_1R completely abolished binding of AngII and its analog [Sar^1, Ile^8]AngII. Noda et al.[45] suggesting that $Lys199^{5.42}$ interaction with $Phe8^{AngII}$ α-carboxyl may be important for the orientation of His6-Pro7-Phe8AngII in mediating receptor agonism. After 200 ns the guanidinium group of $Arg167^{ECL2}$ forms multiple interactions including water mediated bonding with backbone carbonyl groups of $Phe8^{AngII}$, $His6^{AngII}$, and $Ile5^{AngII}$ amounting to 250% of interaction. When $Arg167^{ECL2}$ was mutated, AngII binding is abolished. Therefore, projecting $Arg167^{ECL2}$ into the depth of the

Author Manuscript Author Manuscript Author Manuscript Author Manuscript

orthosteric pocket to support interaction with AngII backbone carbonyls might be critical for shaping the receptor-bound conformation of AngII. We have explored every critical binding pocket residue of AT_1R involved in AngII binding. We did not find significant change in the conformation of $Arg167^{ECL2}$ in AT_1R bound with AngII or olmesartan. Supporting result was observed in our mutagenesis and crystal structure experiments (Table S1).

The NH_2-backbone amide of $Asp1^{AngII}$ interacts with $Asp263^{ECL3}$ and $Ser186^{ECL2}$ and the $Asp1^{AngII}$ carboxyl group maintains interaction with $Lys20^{NT}$. Deletion of $Asp1^{AngII}$ reduces the binding affinity slightly and substitution with sarcosine enhances the binding affinity. The $Arg2^{AngII}$ interacts with $Asp281^{7.32}$ validating the SAR studies, which established its importance for the hormone's binding affinity. The $Asp281^{7.32}$ mutation was shown to reduce AngII affinity as well as efficacy.[60] Previous modeling studies also indicate that additional stabilization of this interaction may involve Asp2787.29. During simulation, $Arg2^{AngII}$ appears to form a strong interaction with $Asp1^{AngII}$ as well as Asp17NT. These interactions contributed ≈130% each, implicating their role in binding $Arg2^{AngII}$.

$Phe8^{AngII}$ reaches deep toward the core of the receptor, while $Tyr4^{AngII}$ is positioned near the extracellular entrance of the orthosteric binding-cavity.$Tyr4^{AngII}$ and $Phe8^{AngII}$ are important for agonistic potency, [Ile4, Ile8]-AngII functions as a low affinity antagonist and [Ile4]AngII and [Ile8]AngII are low efficacy partial agonists for AT_1R. Hence, $Tyr4^{AngII}$ and $Phe8^{AngII}$ interactions are critical for activation of the AT_1R (Figure 3). In MDS we observed that dynamic state of $Tyr4^{AngII}$ precludes a stable interaction of this side chain with the receptor.

$Phe8^{AngII}$ is oriented toward $Trp84^{2.60}$ forming a strong $\pi-\pi$ stacking interaction. Also $Trp84^{2.60}$ forms intramolecular interactions with $Leu81^{2.57}$, $Tyr87^{2.63}$, $Thr88^{2.64}$, $Ala104^{3.28}$, and $Arg167^{ECL2}$. $Trp84^{2.60}$ mutation abolished AngII binding because the smaller aliphatic residues introduced alter conformational geometry and disrupt interactions with $Tyr87^{2.63}$ and $Arg167^{ECL2}$. $Tyr92^{ECL1}$ mutation to Ala completely abolished AngII binding. $Tyr92^{ECL1}$ forms hydrophobic interaction with $Pro7^{AngII}$, which is important for the active conformation of the AngII. $Pro7^{AngII}$ substitution with a positively or uncharged residue completely abolishes binding affinity of AngII.

The $Ile288^{7.39}$ side chain is oriented toward $Phe8^{AngII}$ making a van der Waals interaction. Mutation with Ala in this position abolished AngII binding, since the shorter side chain of Ala could not reach $Phe8^{AngII}$ to establish a van der Waals interaction. Mutagenesis further showed that a bulkier $Phe288^{7.39}$ side chain does not significantly affect AngII binding. This observation is consistent with modifications of $Phe8^{AngII}$ such as [Sar1, Ile8]AngII and des-Phe8-heptapeptide, which are devoid of AT_1R agonism.

AngII-Induced Conformational Changes.

Systematic changes observed in AT_1R conformation upon AngII binding in our MDS mimic structures of the active-like state GPCRs. In the following sections, we describe the time sequence of structural changes connecting AngII binding site to different cytoplasmic microswitches (Table 1).

Author Manuscript Author Manuscript Author Manuscript Author Manuscript

Breaking Primary Constraint (Asn111$^{3.35}$-Asn295$^{7.46}$ H-Bond).—The most important agonism determinant is Phe8^{AngII} side chain which orientates toward a cluster formed by Tyr35$^{1.39}$, Trp84$^{2.60}$, Pro285$^{7.36}$, Ile288$^{7.39}$, and Tyr292$^{7.43}$ throughout the 1000 ns MDS. The Phe8^{AngII} aromatic side chain "grasps" Ile288$^{7.39}$ in van der Waals attraction within ~100 ns (Figure 4), and this "grasp" pulls the aromatic side chain of Tyr292$^{7.43}$, resulting in breakage of the interhelical H-bond between Tyr292$^{7.43}$−OH and the backbone carbonyl of Val108$^{3.32}$ in ~200 ns which in turn breaks interhelical H-bonds between Asn111$^{3.35}$-Asn295$^{7.46}$ in ~500 ns. Interestingly, equivalent intrahelical H-bonds between TM3-TM7 are absent in AT_2R.[63]The AT_2R structure (PDB id: 5unf) resembles active like GPCRs and it has a Phe residue at TM$^{7.43}$ position that is equivalent to Tyr292$^{7.43}$ in AT_1R. This evidence further supports the conclusion that MDS produced an active-like state of AT_1R.

In contrast, binding olmesartan establishes independent interaction with both Ile288$^{7.39}$ and Tyr292$^{7.43}$ and consequently stabilizes the TM7-TM3 interhelical H-bonds between Tyr292$^{7.43}$-OH-Val108$^{3.32}$ and Asn111$^{3.35}$-Asn295$^{7.46}$ (Figures 5, S6, and S7). In support of this finding, independent studies have shown that nonpeptide AT_1R antagonists show reduced binding affinity to active like state of AT_1R.[63,64] MD simulations with -Ile8^{AngII}, -Ala8^{AngII}, and -Gly8^{AngII} indicated that the aliphatic side chains replacing Phe8^{AngII} systematically decrease interaction with Ile288$^{7.39}$ which is also validated by the agonist-efficacy experimental data shown in Figure S8.

The disruption of the Asn111$^{3.35}$-Asn295$^{7.46}$ bond being central to AT_1R activation is well-documented: (i) stable interhelical H-bonds between Asn111$^{3.35}$-Asn295$^{7.46}$ are confirmed in ARB-bound AT_1R crystal structures;[13,14] (ii) Asn111$^{3.35}$ mutation to smaller residues Gly, Ala, Ser, and Cys constitutively activate AT_1R;[47,60,65–67] (iii) Asn295$^{7.46}$ to Ser mutation mimics this effect;[64] and (iv) long-range effects of mutations destabilizing Asn111$^{3.35}$-Asn295$^{7.46}$ bond also cause constitutive activation.[57] To further examine, we modeled Asn111Gly$^{3.35}$ mutant of AT_1R and found that the model coordinates matched the active-like-state AT_2R structure better than inactive state AT_1R structure. Substitution of larger side chains, such as the Trp111$^{3.35}$ produced the most inactive AT_1R mutant.[49] The residues involved are conserved in AT_2R, suggesting that the same mechanism may be involved in AngII activation of AT_2R.

Mechanism of TM-Bundle Entropy.—Interhelical polar interaction networks involving conserved residues, Asn46$^{1.50}$, Asp74$^{2.60}$, Asn295$^{7.46}$, and Asn298$^{7.49}$ are rearranged. The Tyr292$^{7.43}$ side chain forms $\pi-\pi$ stacking with Phe77$^{2.53}$ and the Asn111$^{3.35}$-Asn295$^{7.46}$ H-bond interacts with Asp74$^{2.50}$ in the AngII bound state. When the Asn111$^{3.35}$-Asn295$^{7.46}$ H-bond breaks, the Asn295$^{7.46}$ interacts strongly with Asp74$^{2.50}$ and Asn46$^{1.50}$. The weakening of TM7-TM3 interaction sways the side chain of Leu112$^{3.36}$ toward Lys199$^{5.42}$. In a previous MDS study, Cabana et al.[49] compared constitutively active Gly111$^{3.35}$ mutant with the inactive Trp111$^{3.35}$ mutant. Although the Asn111$^{3.35}$-Asn295$^{7.46}$ H-bond is broken in both of these mutants, the activation switch to Asn295$^{7.46}$-Asp74$^{2.50}$-Asn46$^{1.50}$ H-bonds was not observed in the Trp111$^{3.35}$ mutant. Instead, Asp74$^{2.50}$ stably interacted with Trp111$^{3.35}$. In the constitutively active Gly111$^{3.35}$ mutant, they observed H-bond between Asp74$^{2.50}$-Asn46$^{1.50}$. Therefore, orderly rearrangement of interhelical network coordinated

Author Manuscript Author Manuscript Author Manuscript Author Manuscript

with Asn111$^{3.35}$-Asn295$^{7.46}$ interaction in the AT_1R are critical steps in activation. AngII binding also perturbed another important hydrogen bonding network involving Asp74$^{2.50}$, with Ser109$^{3.33}$, Tyr113$^{3.37}$ and Cys296$^{7.47}$ that is conserved among class A GPCRs (Figure S9). Biochemical experiments showed that agonist-activation of AT_1R alters the orientation of TM2, reducing its interaction with TM7. The Asp74$^{2.50}$ and Phe77$^{2.53}$ side chains buried in AT_1R become solvent exposed when AngII-binds.[61,68,69]

In addition to the networks in the AngII binding pocket, extensive H-bond network linking the orthosteric ligand pocket and the G-protein-binding cleft also rearrange in the active-like state. In this network, polar residues are conserved as documented in family A GPCR structures and may involve water molecules and a sodium ion as discovered in the high-resolution inactive-state structure of a few GPCRs.[10,11,40] Since involvement of allosteric sodium is not experimentally confirmed in AT_1R, we did not include a sodium ion in our MDS analysis. However, the cytoplasmic H-bond networks can be traced to the side chains of Asp74$^{2.50}$, Asn111$^{3.35}$, Trp253$^{6.48}$, and Asn295$^{7.46}$ that could be involved in coordination of a sodium ion. As discussed below the polar networks extend from CWxP^{TM6} motif to the cytoplasmic surface involving microswitches, the DRY^{TM3}, Yx7K(R)^{TM5}, and NPxxY^{TM7} sequences.

Motion of Trp253$^{6.48}$.—Trp253$^{6.48}$ is part of the CWxP motif, a rotamer toggle switch which leads to the opening of G protein cleft in class A GPCRs. This highly conserved amino acid residue is located on the floor of the ligand pocket and adjacent to the conserved Pro2556.50. No significant change in orientation of Pro255$^{6.50}$ is observed in our MD simulation. In the AngII activated state the orientation of Trp253$^{6.48}$ side chain tilts intracellular toward His256$^{6.51}$ and Phe249$^{6.44}$, which are in close interactions with the cluster of aromatic residues Phe204$^{5.47}$, Phe208$^{5.51}$, and Tyr292$^{7.43}$ (Figure 6). Of these, His256$^{6.51}$ is a key coupling residue as mutations in this residue uncouple AT_1R agonist binding and G protein activation.[44,45] While the C_α torsion remained constant, the Trp253$^{6.48}$ side chain torsion was stabilized in ~200 ns in the AngII-bound state and in 500 ns in the Olmesartan-bound states (Figure S10). The nature of CWxP conformational changes is not identical in eight agonist or G-protein bound active state GPCR structures in PDB (PDB ids: 2YDV, 3SN6, 5GLH, 4MQS, 5C1M, 3PQR, 5YNF). However, the motion observed in our simulation best matched with ET_BR and A_2ARs (Figure S10B). The hydrophobic interaction between Trp253$^{6.48}$ and Phe249$^{6.44}$ is also observed in the active-like states of NTSR1 and μ-opioid receptor.

Motion of Tyr215$^{5.58}$.—Tyr215$^{5.58}$ is located closer to the cytoplasmic end of TM5 and is part of the Yx7K^{TM5} motif. Highly conserved throughout the GPCR family, the Tyr side chain at this location may serve the need for the polarity and the bulky hydrophobic ring system to ensure requirements for an efficient stabilizing motif in the active states of GPCRs.[70,71] In crystal structures of GPCRs, Tyr215$^{5.58}$ forms an H-bond with Arg126$^{3.50}$ side chain of the DRY motif in the active state. In AT_1R, this bonding is not observed throughout the simulation. Instead we observed a strong and continuous interaction of Tyr215$^{5.58}$ with Leu119$^{3.43}$ which helps TM3 and TM5 remain closer. But in the active state, the Tyr215$^{5.58}$ side chain moves toward the surface of the protein and forms $\pi-\pi$

Author Manuscript Author Manuscript Author Manuscript Author Manuscript

interaction with Trp219$^{5.62}$ which makes the intracellular region of TM5 less flexible (Figure 7 and S11).

DRY$^{3.51}$ Switch.—The Asp125$^{3.49}$-Arg126$^{3.50}$-Tyr127$^{3.51}$ located at the cytoplasmic end of TM3 in AT_1R is a highly conserved motif in GPCRs and often called an “ionic-lock”, restricting G protein interaction. In the current simulation we observed a distinct difference in orientation and H-bond networking of Arg126$^{3.50}$. In the inactive state, Arg126$^{3.50}$ is involved in stable intrahelical salt bridge with Asp125$^{3.49}$ which stabilizes the intracellular portion of TM3 to remain compact. This observation was also reported by Matsoukas et al.[38] Figure 8 depicts the conformation of this microswitch in the active state. The side chain of Arg126$^{3.50}$ moves toward TM6 and forms an H-bond with Asp237$^{6.32}$ (Figure S12). These rearrangements could be the beginning of opening of the groove for binding G-protein.

NPxxY$^{TM7.53}$ Motif and Helix-8.—The Asn298$^{7.49}$-Pro299$^{7.50}$-Leu$^{7.51}$-Glu$^{7.52}$-Tyr302$^{7.53}$ motif is also highly conserved in GPCRs. Mutations targeting this motif reduce G protein activation by AT_1R.[61,72] During AngII activation, the NPxxY^{TM7} moves toward the conserved Tyr215$^{5.58}$ forming a hydrogen-bond network with Asn298$^{7.51}$, Tyr302$^{7.53}$, and Leu119$^{3.43}$ (Figure 9). A similar hydrogen-bond network was reported in activated structures of rhodopsin, β_2AR, and M_2R. The movements associated with NPxxY also contribute to opening the groove for G-protein binding.

A ~15 Å movement of helix-8 toward the membrane is observed in AngII-bound AT_1R, but not in the olmesartan-bound AT_1R. The secondary structure of helix-8 changes from α helix to unstructured in AngII bound state (Figure 9). Another dynamic feature observed in most activated GPCRs including AT_1R is the increase of the Tyr302$^{7.53}$-Tyr112$^{8.53}$ distance, indicating TM7-helix-8 conformational rearrangement. This distance increased gradually in MD simulations after the first 20 ns and remained stable for the rest of the trajectory. Large changes in helix-8 conformation are reported in agonist-bound μ-opioid receptor.[73]

DISCUSSION

Delineating the molecular mechanics involved in the opening of G protein binding cleft when AT_1R engages AngII is an important advancement. Without MDS analysis, visualizing the dynamics of receptor activation would be difficult while accounting for AngII-analog SAR data, molecular pharmacology data, receptor mutagenesis data, and 3D-structure data. MDS analysis indicated that AT_1R conforms to the general paradigm of conformational modulation by ligands. The agonists promote accumulation of the activated state and the inverse agonists depleted the basal state with minor structural changes (Figure 1). The activated state accumulated spontaneously in the constitutively active Asn111Gly$^{3.35}$ mutant suggesting that the wild-type AT_1R activation must involve agonist-dependent repositioning of Asn111$^{3.35}$ side chain. The Asn111$^{3.35}$-Asn295$^{7.46}$ bond is the prime constraining interaction in AT_1R. When AngII binds this bond is broken indirectly through strain induced by the van der Waals attraction of Ile288$^{7.39}$ toward the well-known agonism-specifying Phe8^{AngII} (Figures 3−5). This is a novel GPCR activation mechanism unlike the agonist trigger mechanisms in well-known GPCRs. For instance, rhodopsin photoactivation which serves as a prototype includes two triggering events, protonation breakage of the buried salt-

Author Manuscript Author Manuscript Author Manuscript Author Manuscript

bridge linking TM7 (retinal-Lys Schiff-base) to TM3 (counterion) and the resulting mechanical motion of functional microdomains.[12,74] In other ligand activated GPCRs different variations of a Lewis acid/base interaction chemical mechanisms operate. For instance, in β-adrenergic receptor, TM3-TM7 lock is a hydrogen bond between$Tyr^{7.35}$-$Asp^{3.29}$ which interacts with protonated quaternary nitrogen in adrenergic ligands and networked with an $Asn^{7.32}$ residue.[75,76] In activating S1P1R, the lyso-phospholipid sphingosine 1-phosphate receptor, the zwitterionic phosphonate and primary amine groups respectively bond with $Arg^{7.35}$ and $Glu^{3.29}$.[77] Thus, release of the TM3-TM7 ionic-lock is suggested to be the first agonist activation step in GPCRs.[74] However, a general GPCR mechanism for breaking prime constraint remains unclear especially for peptide GPCRs until now.

The chemical nature of interactions of AngII and ARBs with the orthosteric pocket is fundamental to pharmacological outcomes, i.e., agonism and inverse-agonism. MDS analysis indicated that inverse-agonist (olmesartan) binding stabilizes multiple TM3-TM7 interactions and dampens intrinsic motion of helices and motifs of AT_1R (Table 1, Figures 6−9 and S6− S12). In addition, insights regarding the differing roles of critical residues are revealed. For example, in the activated state $Arg167^{ECL2}$ establishes multiple interactions with the backbone carbonyl groups of AngII, morphing its receptor bound conformation. However, $Arg167^{ECL2}$ binds the acidic pharmacophore groups at either ends of inverse-agonists, inhibiting residue rearrangements locally in the orthosteric pocket as well as globally in TM and cytoplasmic domains in the inactive-state (Figures 3 and S5).

Receptor bound conformation or the preferred conformation of a hormone peptide provides critical structural information for designing selective pharmaceutical scaffolds for a GPCR. The AngII structure in solution shows a bioactive γ-turn. Cyclic AngII analogs which restrain this conformation increase potency.[78,79] Specific spatial alignment of aromatic residues in AngII, Tyr-hydroxyl (Y4), His-imidazole (H6), and Phe-benzyl (F8) in this conformation maybe important.[80,81] Hormone peptides, AngII (DRV$\underline{Y}^4\underline{IH}^6\underline{PF}^8$), AngIII (RV$\underline{Y}^4\underline{IH}^6\underline{PF}^8$), and AngIV (V$\underline{Y}^4\underline{IH}^6\underline{PF}^8$) which preserve the turn-motif are capable of modulating blood pressure via activating AT_1R. The pose of AngII in our MDS analysis is consistent with spatial alignment of Tyr (Y4), His (H6), and Phe(F8). Additionally, $Phe8^{AngII}$ substitution with Ile and Gly, as well as its deletion (des-$Phe8^{AngII}$) affect binding and activation. As shown in Figure S7, Ang1–7(DRVY^4IH^6P) with either unstable or absence of the bioactive γ-turn conformation binds poorly and may activate AT_1R at nonphysiological concentrations which is also consistent with its poor MM/GBSA scores from IFD and MDS. Aromatic side chain of $Phe8^{AngII}$ helps to project toward the $Ile288^{7.39}$. Substitution with nonaromatic residues (Ile, Gly, or Ala) produce a different conformation in which the side chain moves toward the ECL2 region.

The design of currently used ARBs to mimic the $\underline{Y}^4\underline{IH}^6\underline{PF}^8$ motif in AngII is confirmed by MDS analysis as well as in previous studies.[19,28,82] This knowledge will be useful in designing better AT_1R-selective scaffolds. Development of next generation AT_1R agonists and antagonists in terms of differences in functional selectivity and tissue tropism has important clinical implications. Given that a significant number of patients are currently

Author Manuscript Author Manuscript Author Manuscript Author Manuscript

prescribed ARBs for indications beyond blood pressure reduction, it is important to know the mechanism of action of these drugs at the receptor level.

To our knowledge, this is the first report detailing activating structural dynamics of a clinically important peptide hormone GPCR. There are ~135 human GPCRs responding to endogenous peptide/protein ligands. Static structures of peptide-activated NTR1, ET_BR, GLPR1 and opioid receptors[2,83,84] are documented. Despite this progress the specific interactions that trigger activation of peptide GPCRs are not easy to decipher. Hence MDS analysis starting with human AT_1R crystal structure described here should prove a useful model for gaining insights into the activation mechanism of peptide GPCRs and drug action. Energy-based models allow characterization of side-chain and backbone shift in the pocket as well as provide a 3D framework of determinants of agonism or inverse agonism essential for rational drug discovery. Important insights into agonist induced changes, establishing the path from ligand binding to G-protein activation can be gained.

In functioning GPCRs, thermodynamic motions within the protein produce a conformational landscape with discernible functional substates.[85,86] The MDS ensemble frames provide an integrated view of substate dynamics and time evolution of receptors from inactive to basal to activated states (Figures 2−9). We observed that the orthosteric pocket and cytoplasmic domain where signal transducer molecules converge are semi-independent. The cytoplasmic domain harbors conserved motifs DRY^{TM3}, $Yx7K^{TM5}$, $NPxxY^{TM7}$, and helix-8. These microswitches were originally described in rhodopsin,[71] and functional studies in AT_1R demonstrate that a high degree of stability of functional motifs in the inactive state prevents spontaneous receptor activation. Mutagenesis of microswitches either constitutively activate the receptor or interferes with overall signaling. The impetus for activation of cytoplasmic microswitches is transmitted through a network of hydrogen bonds from the conserved $CWxP^{TM6}$ toggle-switch motif. Our MDS study shows critical positioning of this TM6-motif, sharing a hydrogen-bonded network between TM1-TM2-TM3-TM7 which includes the highly conserved $Asp74^{2.50}$ in AT_1R. The CWxP motif is part of the proposed sodium-ion binding site formed with $Asn111^{3.35}$ and $Asn295^{7.46}$.[12,13] Further, it interacts with a cluster of residues, $His256^{6.51}$, $Phe204^{5.47}$, $Phe208^{5.51}$, and $Tyr292^{7.43}$ which are associated with TM6 movement.[36,37] Because of high level of conservation of residues at TM6.44, $TM^{6.48}$, and $TM^{2.50}$, the role of the CWxP motif in AT_1R may be same as in other GPCRs. Recent experimental dynamics study in adenosine A_2R found that the interplay between $TM^{2.50}$ and $TM^{6.48}$ regulated structural dynamics localized at cytoplasmic motifs associated with receptor activation[87] which mimics similar observations made in rhodopsin activation.[88,89]

Time-evolution of changes involving residues, $Ile288^{7.39}$, $Tyr292^{7.43}$, $V108^{3.32}$, $Asn111^{3.35}$, $Asn295^{7.46}$, $Asn46^{1.50}$, $Asp74^{2.50}$, and $Trp253^{6.48}$ suggests a sequential conformational transition model in which disruption of the TM3-TM7 interaction leads to movement of TM6 followed by reorientation of the TM1-TM2-TM3-TM7 interhelical network. Alternative nonlinear transition model as proposed earlier[27] with multiple kinetic scheme to account for native cellular and system-wide conditions is more realistic. Nonlinear transition models do include elements of a linear transition model as has been shown for rhodopsin.[90–92]

Author Manuscript Author Manuscript Author Manuscript Author Manuscript

CONCLUSION

Phe8^{AngII} engages Ile288$^{7.39}$ of AT_1R in van der Waals interaction which by pulling Tyr2927.43 and breaking H-bond with Val108$^{3.32}$ initiates AT_1R activation. This is a novel mechanism unlike those described in prototypical GPCR activation models. Breaking the Asn111$^{3.35}$-Asn295$^{7.46}$ bond relaxes the prime constraint; subsequently Asn295$^{7.46}$ interacts with Asp74$^{2.50}$ and Asn46$^{1.50}$ leading to AngII activation of AT_1R. This change in the molecular network leads to systematic change in the intracellular domain, and these changes may be a necessary for creation of a pocket for G-protein binding. In the olmesartan-bound inactive state, we observed a stable Asn111$^{3.35}$-Asn295$^{7.46}$ H-bond interaction and in addition Asn295$^{7.46}$ interacts with Asp74$^{2.50}$. Capturing and understanding the molecular details of activation of AT_1R by AngII and inhibition by ARBs could lead to better design of novel and more potent drugs targeting AT_1R which could effectively prevent AngII pathogenesis.

MATERIALS AND METHODS

Protein Preparation.

The starting coordinates of AT_1R PDB IDs: 4ZUD, 4YAY] were retrieved from Protein Data Bank (www.rcsb.org) and further modified for Glide docking calculations (Glide, Schrodinger, LLC, NY, USA).[93] For these calculations, energy minimization was applied to the protein using the Protein Preparation Wizard by applying an OPLS3 (Optimized Potentials for Liquid Simulations) force field.[94] Missing segments of loops were filled using Prime, Schrodinger, LLC, during the protein preparation.[95] Progressively weaker restraints applied to only the non-hydrogen atoms and structure refinement was done based on the default protocol of Schrodinger, LLC, NY, USA, as Glide uses the full OPLS3 force field at an intermediate docking stage and is claimed to be more sensitive to geometrical details than other docking tools. The most likely positions of hydroxyl and thiol hydrogen atoms, protonation states, and tautomers of His residues, and Chi “flip” assignments for Asn, Gln, and His residues were selected. Finally, energy minimizations of protein were performed until the average root-mean-square deviation of the non-hydrogen atoms reached 0.3 Å.

Ligand Preparation.

We retrieved AngII crystal structure from Protein Data Bank [PDB ID: 1N9V] and the structure was prepared using LigPrep package from Schrodinger, LLC, NY, USA (LigPrep, 2018)[96] by assigning appropriate bond order. AngII PDB structure was converted to mae format (Maestro, Schrodinger, LLC, NY, USA), geometrically optimized and partial atomic charges were computed. Then, at most, 32 poses were generated with different steric features for the subsequent docking study. Olmesartan structure was also prepared in Ligprep using the protocol described earlier.[28]

Induced Fit Docking (IFD).

Induced fit docking (IFD) (Schrodinger, LLC, NY, USA) was used to dock AngII and olmesartan inside the ligand binding pocket of AT_1R. First, the ligand was docked into a rigid receptor model with scaled-down vdW radii. A vdW scaling of 0.5 was used for both

Author Manuscript Author Manuscript Author Manuscript Author Manuscript

the protein and ligand nonpolar atoms. A constrained energy minimization was carried out on the protein structure, keeping it close to the original crystal structure while removing bad steric contacts. Energy minimization was carried out using the OPLS3 force field with implicit solvation model. The Glide XP mode was used for the initial docking and ligand poses were retained for protein structural refinements. Prime (Schrodinger, LLC, NY, USA) was then used to generate the induced-fit protein−ligand complexes (Prime, Schrodinger, LLC, NY, USA).[97] Each of the structures from the previous step were subjected to sidechain and backbone refinements.[98] All residues with at least one atom located within 4.0 Å of each corresponding ligand pose were included in the Prime refinement. The refined complexes were ranked by Prime energy, and the 20 receptor structures within 30 kcal/mol of the minimum energy structure were passed through for a final round of Glide docking and scoring. In the final step, each ligand was redocked into the top 20 refined structures using Glide XP.

MM/GBSA.

Prime/MM-GBSA was used to predict the free energy of binding between the receptor and the AngII or olmesartan. The binding free energy (ΔG_{bind}) was calculated using Prime.[99] The binding free energy (G_{bind}) is then estimated using the following equation:

$$G_{\text{bind}} = \text{ER:L} - (\text{ER} + \text{EL}) + G_{\text{solv}} + G_{\text{SA}}$$

where ER:L is energy of the complex, ER + EL is the sum of the energies of the ligand and the apo protein, using the OPLS3 force field, and ΔG_{solv} (ΔG_{SA}) is the difference between GBSA solvation energy (surface area energy) of complex and sum of the corresponding energies for the ligand and apoprotein.[100–102]

MD Simulation.

Molecular dynamics (MD) simulations were carried out for AT_1R-AngII and AT_1R-olmesartan complexes using Desmond MD code and the OPLS3 force field[92] for minimization of the system. We ran the MD simulation for 1 μS for each of the complexes. For AT_1R-AngII complex, we repeated the MD simulation six times for both the crystal structures solved for AT_1R (PDB id's: 4ZUD and 4YAY) and two times for the AT_1R-olmesartan complex. Using the Desmond system builder, a 10 Å buffered orthorhombic system with periodic boundary conditions was constructed using a POPC lipid membrane[103–106] and an SPC explicit water solvent. The overall charge was neutralized by 0.15 mol/L NaCl. The simulations were performed in the NPT ensemble with number of elements, pressure, and temperature controlled. The temperature of 300 K and pressure of 1.013 bar were kept constant by coupling the system to a Berendsen thermostat and barostat, which are normal temperature and pressure mimicking the real life environment. An integration step of 2.0 was used, Coulombic interactions were calculated using a cutoff radius of 9.0 Å and long-range electrostatic interactions were calculated using the smooth particle mesh Ewald method.[107] Before each MD simulation, a default Desmond membrane protein relaxation protocol was applied.[108] To monitor protein stability and conformational fluctuations throughout the simulations, we computed backbone RMSDs after least-squares

Author Manuscript Author Manuscript Author Manuscript Author Manuscript

fitting to the starting structure. This was done for the entire protein and transmembrane α-helices. The trajectory was selected when the system is fully equilibrated and the RMSD reached its plateau. Statistical analyses are based on the structural ensemble from each cluster. Clustering of trajectory was performed using RMSD clustering tool of Schrodinger software package. Five clusters were generated and average structures were generated from each cluster. Additional structural analyses were further performed using these average structures. All the figures were generated using PyMol (The PyMOL Molecular Graphics System, Version 2.0 Schrödinger, LLC). The volume of the binding pocket was calculated using SiteMap, Schrödinger Release 2018–2: SiteMap, Schrödinger, LLC, New York, NY, 2018. Five representative structure of AT_1R-AngII were generated from the MDS trajectory and average value was reported.

^{125}I-AngII Competition Binding Analysis.

The detailed procedure is described in previous reports from our laboratory.[12,55] Ligand binding was analyzed using membranes prepared from HEK293T cells expressing wild-type HA-AT_1R as described earlier and suspended in membrane binding buffer (140 mMNaCl, 5.4 mMKCl, 1 mM EDTA, 0.006% bovine serum albumin, 25 mMHEPES, pH 7.4). A 10 μg of homogeneous cell membrane was used per well. Competition binding assays were performed under equilibrium conditions, with 2 nM radioligand (^{125}I-AngII purchased from Dr. Robert Speth, University of Mississippi) and concentrations of the competing ligand ranging between 0.04 and 1000 nM. Binding reaction was terminated by filtering the binding mixture through Whatman GF/C glass fiber filters, washed with buffer (20 mMsodium phosphate, 100 mMNaCl, 10 mM MgCl2, 1 mMEGTA, pH 7.2). The bound ligand concentration was determined as the counts/min (MicroBeta2 Plate Counter, PerkinElmer Life Sciences). Nonspecific binding was measured in the presence of 10^5 M ^{127}I-AngII (Bachem). The binding kinetics were analyzed by the nonlinear curve-fitting program GraphPad Prism 5. The means ± SE for the IC_{50} values were calculated.

Comparative Agonism by Intracellular Calcium Levels.

Calcium levels were measured using FLIPR_ calcium 5 assay kit (Molecular Devices) as described previously.[12,13,55] The HA-AT_1R expressing cells were seeded at a density of 100 000 cells/well in a 96-well clear bottom black plate. Following serum starvation, calcium-sensitive dye was added to the cells. The Flipper instrument was programmed in FLEX mode to add ligands (0.04 and 1000 nM concentration) to the cells and to monitor the fluorescence before and after adding the ligands. The dose−response curves were plotted and percent agonism was calculated assuming 100% stimulation by AngII.

Supplementary Material

Refer to Web version on PubMed Central for supplementary material.

Acknowledgments

Funding

This work was supported by National Institutes of Health Grants HL132351 and R01HL142091 and LRI Chair's Innovative Research Award to S.S.K.

Author Manuscript Author Manuscript Author Manuscript Author Manuscript

REFERENCES

(1). Hauser AS; Chavali S; Masuho I; Jahn LJ; Martemyanov KA; Gloriam DE; Babu MM Pharmacogenomics of GPCR Drug Targets. Cell 2018, 172, 41–54.e19. [PubMed: 29249361]

(2). Takeda S; Kadowaki S; Haga T; Takaesu H; Mitaku S Identification of G Protein-Coupled Receptor Genes From The Human Genome Sequence. FEBS Lett 2002, 520, 97–101. [PubMed: 12044878]

(3). Fredriksson R; Lagerstrom MC; Lundin LG; Schioth HB The G-protein-Coupled Receptors in the Human Genome form Five Main Families. Phylogenetic analysis, paralogon groups, and finger prints. Mol. Pharmacol 2003, 63, 1256–1272. [PubMed: 12761335]

(4). Salon JA; Lodowski DT; Palczewski K The Significance of G Protein-Coupled Receptor Crystallography for Drug Discovery. Pharmacol Rev 2011, 63, 901–937. [PubMed: 21969326]

(5). Hauser AS; Attwood MM; Rask-Andersen M; Schioth HB; Gloriam DE Trends In GPCR Drug Discovery: New Agents, Targets and Indications. Nat. Rev. Drug Discovery 2017, 16, 829–842. [PubMed: 29075003]

(6). Wang W; Qiao Y; Li Z New Insights into Modes of GPCR Activation. Trends Pharmacol. Sci 2018, 39, 367–386. [PubMed: 29395118]

(7). Kobilka BK Gprotein Coupled Receptor Structure and Activation. Biochim. Biophys. Acta, Biomembr 2007, 1768, 794–807.

(8). Rosenbaum DM; Rasmussen SG; Kobilka BK The Structure and Function of G-Protein-Coupled Receptors. Nature 2009, 459, 356–363. [PubMed: 19458711]

(9). Park PS; Lodowski DT; Palczewski K Activation of G Protein-Coupled Receptors: Beyond Two-State Models and Tertiary Conformational Changes. Annu. Rev. Pharmacol. Toxicol 2008, 48, 107–141. [PubMed: 17848137]

(10). Cherezov V; Rosenbaum DM; Hanson MA; Rasmussen SG; Thian FS; Kobilka TS; Choi HJ; Kuhn P; Weis WI; Kobilka BK; Stevens RC High-Resolution Crystal Structure of An Engineered Human Beta2-Adrenergic G Protein-Coupled Receptor. Science 2007, 318, 1258–1265. [PubMed: 17962520]

(11). Ring AM; Manglik A; Kruse AC; Enos MD; Weis WI; Garcia KC; Kobilka BK Adrenaline-Activated Structure of Beta2-Adrenoceptor Stabilized By An Engineered Nanobody. Nature 2013, 502, 575–579. [PubMed: 24056936]

(12). Lin SW; Han M; Sakmar TP Analysis of Functional Micro Domains of Rhodopsin. Methods Enzymol 2000, 315, 116–130. [PubMed: 10736698]

(13). Zhang H; Unal H; Desnoyer R; Han GW; Patel N; Katritch V; Karnik SS; Cherezov V; Stevens RC Structural Basis for Ligand Recognition and Functional Selectivity at Angiotensin Receptor. J. Biol. Chem 2015, 290, 29127–29139. [PubMed: 26420482]

(14). Zhang H; Unal H; Gati C; Han GW; Liu W; Zatsepin NA; James D; Wang D; Nelson G; Weierstall U; Sawaya MR; Xu Q; Messerschmidt M; Williams GJ; Boutet S; Yefanov OM; White TA; Wang C; Ishchenko A; Tirupula KC; Desnoyer R; Coe J; Conrad CE; Fromme P; Stevens RC; Katritch V; Karnik SS; Cherezov V Structure of The Angiotensin Receptor Revealed By Serial Femtosecond Crystallography. Cell 2015, 161, 833–844. [PubMed: 25913193]

(15). Zhang X; Perez-Sanchez H; Lightstone FC A Comprehensive Docking and MM/GBSA Rescoring Study of Ligand Recognition upon Binding Antithrombin. Curr. Top. Med. Chem 2017, 17, 1631–1639. [PubMed: 27852201]

(16). Shihoya W; Nishizawa T; Okuta A; Tani K; Dohmae N; Fujiyoshi Y; Nureki O; Doi T Activation Mechanism of Endothelin ETB Receptor by Endothelin-1. Nature 2016, 537, 363–368. [PubMed: 27595334]

(17). Unger T The Role Of The Renin-Angiotensin System in the Development of Cardiovascular Disease. Am. J. Cardiol 2002, 89, 3A–9A discussion 10A.

(18). Duprez DA Role of the Renin-Angiotensin-Aldosterone System in Vascular Remodeling And Inflammation: A Clinical Review. J. Hypertens 2006, 24, 983–991. [PubMed: 16685192]

(19). Pacurari M; Kafoury R; Tchounwou PB; Ndebele K The Renin-Angiotensin-Aldosterone System in Vascular Inflammation and Remodeling. Int. J. Inflammation 2014, 2014, 689360.

Author Manuscript Author Manuscript Author Manuscript Author Manuscript

(20). Karnik SS; Unal H; Kemp JR; Tirupula KC; Eguchi S; Vanderheyden PM; Thomas WG International Union of Basic and Clinical Pharmacology. XCIX. Angiotensin Receptors: Interpreters of Pathophysiological Angiotensinergic Stimuli [corrected]. Pharmacol. Rev 2015, 67, 754–819. [PubMed: 26315714]

(21). Shenoy SK; Lefkowitz RJ Angiotensin II-Stimulated Signaling Through G Proteins and Beta-Arrestin. Sci. Signaling 2005, 2005, cm14.

(22). Balla T; Varnai P; Tian Y; Smith RD Signaling Events Activated by Angiotensin II Receptors: What Goes Before and After the Calcium Signals. Endocr. Res 1998, 24, 335–344. [PubMed: 9888505]

(23). Rodrigues-Ferreira S; Nahmias C G-Protein Coupled Receptors of the Renin-Angiotensin System: New Targets Against Breast Cancer? Front. Pharmacol 2015, 6, 24. [PubMed: 25741281]

(24). Yee DK; Suzuki A; Luo L; Fluharty SJ Identification of Structural Determinants for G Protein-Independent Activation of Mitogen-Activated Protein Kinases in the Seventh Transmembrane Domain of the Angiotensin II Type 1 Receptor. Mol. Endocrinol 2006, 20, 1924–1934. [PubMed: 16556732]

(25). Doan TN; Ali MS; Bernstein KE Tyrosine Kinase Activation by the Angiotensin II Receptor in the Absence of Calcium Signaling. J. Biol. Chem 2001, 276, 20954–20958. [PubMed: 11319216]

(26). Mehta PK; Griendling KK Angiotensin II Cell Signaling: Physiological and Pathological Effects in the Cardiovascular System. Am. J. Physiol Cell Physiol 2007, 292, C82–97. [PubMed: 16870827]

(27). Higuchi S; Ohtsu H; Suzuki H; Shirai H; Frank GD; Eguchi S Angiotensin Ii Signal Transduction Through The AT1 Receptor: Novel Insights into Mechanisms and Pathophysiology. Clin. Sci 2007, 112, 417–428. [PubMed: 17346243]

(28). Unal H; Karnik SS Domain Coupling in GPCRS: The Engine for Induced Conformational Changes. Trends Pharmacol. Sci 2012, 33, 79–88. [PubMed: 22037017]

(29). Singh KD; Unal H; Desnoyer R; Karnik SS Divergent Spatiotemporal Interaction of Angiotensin Receptor Blocking Drugs with Angiotensin Type 1 Receptor. J. Chem. Inf. Model 2018, 58, 182–193. [PubMed: 29195045]

(30). Lu M; Wu B Structural Studies of G Protein-Coupled Receptors. IUBMB Life 2016, 68, 894–903. [PubMed: 27766738]

(31). Sanchez-Reyes OB; Cooke ALG; Tranter DB; Rashid D; Eilers M; Reeves PJ; Smith SO G Protein-Coupled Receptors Contain Two Conserved Packing Clusters. Biophys. J 2017, 112, 2315–2326. [PubMed: 28591604]

(32). Fredriksson R; Hoglund PJ; Gloriam DE; Lagerstrom MC; Schioth HB Seven Evolutionarily Conserved Human Rhodopsin G Protein-Coupled Receptors Lacking Close Relatives. FEBS Lett 2003, 554, 381–388. [PubMed: 14623098]

(33). Venkatakrishnan AJ; Deupi X; Lebon G; Heydenreich FM; Flock T; Miljus T; Balaji S; Bouvier M; Veprintsev DB; Tate CG; Schertler GF; Babu MM Diverse Activation Pathways in Class A GPCRS Converge Near the G-Protein-Coupling Region. Nature 2016, 536, 484–487. [PubMed: 27525504]

(34). Venkatakrishnan AJ; Deupi X; Lebon G; Tate CG; Schertler GF; Babu MM Molecular Signatures of G-Protein-Coupled Receptors. Nature 2013, 494, 185–194. [PubMed: 23407534]

(35). Fillion D; Cabana J; Guillemette G; Leduc R; Lavigne P; Escher E Structure of The Human Angiotensin II Type 1 (AT1) Receptor Bound to Angiotensin II From Multiple Chemo-selective photo probe Contacts Reveals A Unique Peptide Binding Mode. J. Biol. Chem 2013, 288, 8187–8197. [PubMed: 23386604]

(36). Clement M; Martin SS; Beaulieu ME; Chamberland C; Lavigne P; Leduc R; Guillemette G; Escher E Determining the Environment of The Ligand Binding Pocket of the Human Angiotensin II Type I (hAT1) Receptor Using the Methionine Proximity Assay. J. Biol. Chem 2005, 280, 27121–27129. [PubMed: 15890659]

(37). Cabana J; Holleran B; Leduc R; Escher E; Guillemette G; Lavigne P Identification of Distinct Conformations of the Angiotensin-II Type 1 Receptor Associated with the Gq/11 Protein

Author Manuscript Author Manuscript Author Manuscript Author Manuscript

Pathway and the beta-Arrestin Pathway Using Molecular Dynamics Simulations. J. Biol. Chem 2015, 290, 15835–15854. [PubMed: 25934394]

(38). Matsoukas MT; Potamitis C; Plotas P; Androutsou ME; Agelis G; Matsoukas J; Zoumpoulakis P Insights into AT1 Receptor Activation Through AngII Binding Studies. J. Chem. Inf. Model 2013, 53, 2798–2811. [PubMed: 24053563]

(39). Lebon G; Warne T; Edwards PC; Bennett K; Langmead CJ; Leslie AG; Tate CG Agonist-Bound Adenosine A2a Receptor Structures Reveal Common Features of GPCR Activation. Nature 2011, 474, 521–525. [PubMed: 21593763]

(40). Rasmussen SG; DeVree BT; Zou Y; Kruse AC; Chung KY; Kobilka TS; Thian FS; Chae PS; Pardon E; Calinski D; Mathiesen JM; Shah ST; Lyons JA; Caffrey M; Gellman SH; Steyaert J; Skiniotis G; Weis WI; Sunahara RK; Kobilka BK Crystal Structure of the Beta2 Adrenergic Receptor-Gs Protein Complex. Nature 2011, 477, 549–555. [PubMed: 21772288]

(41). Kruse AC; Ring AM; Manglik A; Hu J; Hu K; Eitel K; Hubner H; Pardon E; Valant C; Sexton PM; Christopoulos A; Felder CC; Gmeiner P; Steyaert J; Weis WI; Garcia KC; Wess J; Kobilka BK Activation and Allosteric Modulation of a Muscarinic Acetylcholine Receptor. Nature 2013, 504, 101–106. [PubMed: 24256733]

(42). Huang W; Manglik A; Venkatakrishnan AJ; Laeremans T; Feinberg EN; Sanborn AL; Kato HE; Livingston KE; Thorsen TS; Kling RC; Granier S; Gmeiner P; Husbands SM; Traynor JR; Weis WI; Steyaert J; Dror RO; Kobilka BK Structural Insights into Micro-Opioid Receptor Activation. Nature 2015, 524, 315–321. [PubMed: 26245379]

(43). Choe HW; Kim YJ; Park JH; Morizumi T; Pai EF; Krauss N; Hofmann KP; Scheerer P; Ernst OP Crystal Structure of Metarhodopsin II. Nature 2011, 471, 651–655. [PubMed: 21389988]

(44). Miura S; Feng YH; Husain A; Karnik SS Role of Aromaticity of Agonist Switches of Angiotensin II in the Activation of the AT1 Receptor. J. Biol. Chem 1999, 274, 7103–7110. [PubMed: 10066768]

(45). Noda K; Feng YH; Liu XP; Saad Y; Husain A; Karnik SS The Active State of the At1 Angiotensin Receptor is Generated by Angiotensin II Induction. Biochemistry 1996, 35, 16435–16442. [PubMed: 8987975]

(46). Nikiforovich GV; Zhang M; Yang Q; Jagadeesh G; Chen HC; Hunyady L; Marshall GR; Catt KJ Interactions Between Conserved Residues in Transmembrane Helices 2 and 7 During Angiotensin AT1 Receptor Activation. Chem. Biol. Drug Des 2006, 68, 239–249. [PubMed: 17177883]

(47). Auger-Messier M; Turgeon ES; Leduc R; Escher E; Guillemette G The Constitutively Active N111G-AT1 Receptor for Angiotensin II Modifies the Morphology and Cytoskeletal Organization of Hek-293 Cells. Exp. Cell Res 2005, 308, 188–195. [PubMed: 15896777]

(48). Bhuiyan MA; Hossain M; Miura S; Nakamura T; Ozaki M; Nagatomo T Constitutively Active Mutant N111G of Angiotensin II Type 1 (AT(1)) Receptor Induces Homologous Internalization Through Mediation of AT(1)-receptor Antagonist. J. Pharmacol. Sci 2009, 111, 227–234. [PubMed: 19881223]

(49). Cabana J; Holleran B; Beaulieu ME; Leduc R; Escher E; Guillemette G; Lavigne P Critical Hydrogen Bond Formation for Activation of the Angiotensin II Type 1 Receptor. J. Biol. Chem 2013, 288, 2593–2604. [PubMed: 23223579]

(50). Wilkes BC; Masaro L; Schiller PW; Carpenter KA Angiotensin II vs its Type I Antagonists: Conformational Requirements for Receptor Binding Assessed From NMR Spectroscopic and Receptor Docking Experiments. J. Med. Chem 2002, 45, 4410–4418. [PubMed: 12238921]

(51). Holloway AC; Qian H; Pipolo L; Ziogas J; Miura S; Karnik S; Southwell BR; Lew MJ; Thomas WG Side-Chain Substitutions Within Angiotensin II Reveal Different Requirements for Signaling, Internalization, and Phosphorylation of Type 1A Angiotensin Receptors. Mol. Pharmacol 2002, 61, 768–777. [PubMed: 11901215]

(52). Zimmerman B; Beautrait A; Aguila B; Charles R; Escher E; Claing A; Bouvier M; Laporte SA Differential Beta-Arrestin-Dependent Conformational Signaling and Cellular Responses Revealed by Angiotensin Analogs. Sci. Signaling 2012, 5, ra33.

Author Manuscript Author Manuscript Author Manuscript Author Manuscript

(53). Noda K; Saad Y; Karnik SS Interaction of Phe8 of Angiotensin II with Lys199 and His256 of AT1 Receptor in Agonist Activation. J. Biol. Chem 1995, 270, 28511–28514. [PubMed: 7499361]

(54). Auger-Messier M; Clement M; Lanctot PM; Leclerc PC; Leduc R; Escher E; Guillemette G The Constitutively Active N111G-AT1 Receptor for Angiotensin II Maintains a High Affinity Conformation Despite Being Uncoupled From Its Cognate G Protein Gq/11alpha. Endocrinology 2003, 144, 5277–5284. [PubMed: 12960024]

(55). Schambye HT; Hjorth SA; Bergsma DJ; Sathe G; Schwartz TW Differentiation Between Binding Sites for Angiotensin II and Nonpeptide Antagonists on the Angiotensin II Type 1 Receptors. Proc. Natl. Acad. Sci. U. S. A 1994, 91, 7046–7050. [PubMed: 8041743]

(56). Unal H; Jagannathan R; Bhat MB; Karnik SS Ligand-Specific Conformation of Extracellular Loop-2 in the Angiotensin II Type 1 Receptor. J. Biol. Chem 2010, 285, 16341–16350. [PubMed: 20299456]

(57). Unal H; Jagannathan R; Bhatnagar A; Tirupula K; Desnoyer R; Karnik SS Long Range Effect of Mutations on Specific Conformational Changes in the Extracellular Loop 2 of Angiotensin II Type 1 Receptor. J. Biol. Chem 2013, 288, 540–551. [PubMed: 23139413]

(58). Tirupula KC; Ithychanda SS; Mohan ML; Naga Prasad SV; Qin J; Karnik SS G Protein-Coupled Receptors Directly Bind Filamin A With High Affinity and Promote Filamin Phosphorylation. Biochemistry 2015, 54, 6673–6683. [PubMed: 26460884]

(59). Bihoreau C; Monnot C; Davies E; Teutsch B; Bernstein KE; Corvol P; Clauser E Mutation of Asp74 of the Rat Angiotensin II Receptor Confers Changes in Antagonist Affinities and Abolishes G-Protein Coupling. Proc. Natl. Acad. Sci. U. S. A 1993, 90, 5133–5137. [PubMed: 8506360]

(60). Feng YH; Noda K; Saad Y; Liu XP; Husain A; Karnik SS The Docking of Arg2 of Angiotensin II with Asp281 of AT1 Receptor is Essential for Full Agonism. J. Biol. Chem 1995, 270, 12846–12850. [PubMed: 7759541]

(61). Boucard AA; Roy M; Beaulieu ME; Lavigne P; Escher E; Guillemette G; Leduc R Constitutive Activation of the Angiotensin II Type 1 Receptor Alters the Spatial Proximity of Transmembrane 7 to the Ligand-Binding Pocket. J. Biol. Chem 2003, 278, 36628–36636. [PubMed: 12842881]

(62). Kellici TF; Ntountaniotis D; Kritsi E; Zervou M; Zoumpoulakis P; Potamitis C; Durdagi S; Salmas RE; Ergun G; Gokdemir E; Halabalaki M; Gerothanassis IP; Liapakis G; Tzakos A; Mavromoustakos T Leveraging NMR and X-ray Data of the Free Ligands to Build Better Drugs Targeting Angiotensin II Type 1 G-Protein Coupled Receptor. Curr. Med. Chem 2015, 23, 36–59.

(63). Zhang H; Han GW; Batyuk A; Ishchenko A; White KL; Patel N; Sadybekov A; Zamlynny B; Rudd MT; Hollenstein K; Tolstikova A; White TA; Hunter MS; Weierstall U; Liu W; Babaoglu K; Moore EL; Katz RD; Shipman JM; Garcia-Calvo M; Sharma S; Sheth P; Soisson SM; Stevens RC; Katritch V; Cherezov V Structural Basis for Selectivity and Diversity in Angiotensin II Receptors. Nature 2017, 544, 327–332. [PubMed: 28379944]

(64). Takezako T; Unal H; Karnik SS; Node K Structure-Function Basis of Attenuated Inverse Agonism of Angiotensin II Type 1 Receptor Blockers for Active-State Angiotensin II Type 1 Receptor. Mol. Pharmacol 2015, 88, 488–501. [PubMed: 26121982]

(65). Unal H; Karnik SS Constitutive Activity in the Angiotensin II Type 1 Receptor: Discovery and Applications. Adv. Pharmacol 2014, 70, 155–174. [PubMed: 24931196]

(66). Noda K; Feng YH; Liu XP; Saad Y; Husain A; Karnik SS The Active State of the AT1 Angiotensin Receptor is Generated by Angiotensin II Induction. Biochemistry 1996, 35, 16435–16442. [PubMed: 8987975]

(67). Groblewski T; Maigret B; Larguier R; Lombard C; Bonnafous JC; Marie J Mutation of Asn111 in the Third Transmembrane Domain of the AT1A Angiotensin II Receptor Induces its Constitutive Activation. J. Biol. Chem 1997, 272, 1822–1826. [PubMed: 8999867]

(68). Miura S; Karnik SS Constitutive Activation of Angiotensin II Type 1 Receptor Alters the Orientation of Transmembrane Helix-2. J. Biol. Chem 2002, 277, 24299–24305. [PubMed: 11983705]

Author Manuscript Author Manuscript Author Manuscript Author Manuscript

(69). Miura S; Zhang J; Boros J; Karnik SS TM2-TM7 Interaction in Coupling Movement of Transmembrane Helices to Activation of the Angiotensin II Type-1 Receptor. J. Biol. Chem 2003, 278, 3720–3725. [PubMed: 12446719]

(70). Goncalves JA; South K; Ahuja S; Zaitseva E; Opefi CA; Eilers M; Vogel R; Reeves PJ; Smith SO Highly Conserved Tyrosine Stabilizes the Active State of Rhodopsin. Proc. Natl. Acad. Sci. U. S. A 2010, 107, 19861–19866. [PubMed: 21041664]

(71). Elgeti M; Kazmin R; Heck M; Morizumi T; Ritter E; Scheerer P; Ernst OP; Siebert F; Hofmann KP; Bartl FJ Conserved Tyr223(5.58) plays different roles in the activation and G-protein interaction of rhodopsin. J. Am. Chem. Soc 2011, 133, 7159–7165. [PubMed: 21506561]

(72). Laporte SA; Servant G; Richard DE; Escher E; Guillemette G; Leduc R The tyrosine within the NPXnY motif of the human angiotensin II type 1 receptor is involved in mediating signal transduction but is not essential for internalization. Mol. Pharmacol 1996, 49, 89–95. [PubMed: 8569717]

(73). Sounier R; Mas C; Steyaert J; Laeremans T; Manglik A; Huang W; Kobilka BK; Demene H; Granier S Propagation of Conformational Changes During Mu-Opioid Receptor Activation. Nature 2015, 524, 375–378. [PubMed: 26245377]

(74). Kim JM; Altenbach C; Kono M; Oprian DD; Hubbell WL; Khorana HG Structural Origins of Constitutive Activation in Rhodopsin: Role of the K296/E113 Salt Bridge. Proc. Natl. Acad. Sci. U. S. A 2004, 101, 12508–12513. [PubMed: 15306683]

(75). Dror RO; Arlow DH; Maragakis P; Mildorf TJ; Pan AC; Xu H; Borhani DW; Shaw DE Activation Mechanism of the Beta2-Adrenergic Receptor. Proc. Natl. Acad. Sci. U. S. A 2011, 108, 18684–18689. [PubMed: 22031696]

(76). Trzaskowski B; Latek D; Yuan S; Ghoshdastider U; Debinski A; Filipek S Action of Molecular Switches IN GPCRS-Theoretical and Experimental Studies. Curr. Med. Chem 2012, 19, 1090–1109. [PubMed: 22300046]

(77). Hanson MA; Roth CB; Jo E; Griffith MT; Scott FL; Reinhart G; Desale H; Clemons B; Cahalan SM; Schuerer SC; Sanna MG; Han GW; Kuhn P; Rosen H; Stevens RC Crystal Structure of a Lipid G Protein-Coupled Receptor. Science 2012, 335, 851–855. [PubMed: 22344443]

(78). Murphy KP; Xie D; Garcia KC; Amzel LM; Freire E Structural Energetics of Peptide Recognition: Angiotensin II/Antibody Binding. Proteins: Struct., Funct., Genet 1993, 15, 113–20. [PubMed: 8441749]

(79). Nikiforovich GV; Kao JL; Plucinska K; Zhang WJ; Marshall GR Conformational Analysis of Two Cyclic Analogs of Angiotensin: Implications For the Biologically Active Conformation. Biochemistry 1994, 33, 3591–3598. [PubMed: 8142357]

(80). Nikiforovich GV; Marshall GR Three-Dimensional Recognition Requirements for Angiotensin Agonists: A Novel Solution for an Old Problem. Biochem. Biophys. Res. Commun 1993, 195, 222–228. [PubMed: 8363604]

(81). Rosenstrom U; Skold C; Lindeberg G; Botros M; Nyberg F; Karlen A; Hallberg A A Selective AT2 Receptor Ligand with A Gamma-Turn-Like Mimetic Replacing The Amino Acid Residues 4− 5 Of Angiotensin II. J. Med. Chem 2004, 47, 859–870. [PubMed: 14761188]

(82). Potamitis C; Zervou M; Katsiaras V; Zoumpoulakis P; Durdagi S; Papadopoulos MG; Hayes JM; Grdadolnik SG; Kyrikou I; Argyropoulos D; Vatougia G; Mavromoustakos T Antihypertensive Drug Valsartan in Solution and at the AT1 Receptor: Conformational Analysis, Dynamic NMR Spectroscopy, In Silico Docking, and Molecular Dynamics Simulations. J. Chem. Inf. Model 2009, 49, 726–739. [PubMed: 19256500]

(83). Foord SM Receptor Classification: Post Genome. Curr. Opin. Pharmacol 2002, 2, 561–566. [PubMed: 12324260]

(84). Ghosh E; Kumari P; Jaiman D; Shukla AK Methodological Advances: The Unsung Heroes of the GPCR Structural Revolution. Nat. Rev. Mol. Cell Biol 2015, 16, 69–81. [PubMed: 25589408]

(85). Ramanathan A; Savol A; Burger V; Chennubhotla CS; Agarwal PK Protein Conformational Populations and Functionally Relevant Sub States. Acc. Chem. Res 2014, 47, 149–156. [PubMed: 23988159]

Author Manuscript Author Manuscript Author Manuscript Author Manuscript

(86). Shukla D; Hernandez CX; Weber JK; Pande VS Markov State Models Provide Insights into Dynamic Modulation of Protein Function. Acc. Chem. Res 2015, 48, 414–422. [PubMed: 25625937]

(87). Eddy MT; Lee MY; Gao ZG; White KL; Didenko T; Horst R; Audet M; Stanczak P; McClary KM; Han GW; Jacobson KA; Stevens RC; Wuthrich K Allosteric Coupling of Drug Binding and Intracellular Signaling in the A2A Adenosine Receptor. Cell 2018, 172, 68–80.e12. [PubMed: 29290469]

(88). Lin SW; Sakmar TP Specific Tryptophan UV-Absorbance Changes are Probes of the Transition of Rhodopsin to its Active State. Biochemistry 1996, 35, 11149–11159. [PubMed: 8780519]

(89). Crocker E; Eilers M; Ahuja S; Hornak V; Hirshfeld A; heves M; Smith SO Location of Trp265 in Meta rhodopsin II: Implications for the Activation Mechanism of the Visual Receptor Rhodopsin. J. Mol. Biol 2006, 357, 163–172. [PubMed: 16414074]

(90). Szundi I; Lewis JW; Kliger DS Deriving Reaction Mechanisms from Kinetic Spectroscopy. Application to Late Rhodopsin Intermediates. Biophys. J 1997, 73, 688–702. [PubMed: 9251787]

(91). Zaitseva E; Brown MF; Vogel R Sequential Rearrangement of Interhelical Networks Upon Rhodopsin Activation in Membranes: The Meta II(A) Conformational Sub state. J. Am. Chem. Soc 2010, 132, 4815–4821. [PubMed: 20230054]

(92). Altenbach C; Kusnetzow AK; Ernst OP; Hofmann KP; Hubbell WL High-Resolution Distance Mapping in Rhodopsin Reveals the Pattern of Helix Movement Due to Activation. Proc. Natl. Acad. Sci. U. S. A 2008, 105, 7439–7444. [PubMed: 18490656]

(93). Glide; Schrödinger Release 2018–1; Schrödinger, LLC: New York, NY, 2018.

(94). Harder E; Damm W; Maple J; Wu C; Reboul M; Xiang JY; Wang L; Lupyan D; Dahlgren MK; Knight JL; Kaus JW; Cerutti DS; Krilov G; Jorgensen WL; Abel R; Friesner RA OPLS3: A Force Field Providing Broad Coverage of Drug-like Small Molecules and Proteins. J. Chem. Theory Comput 2016, 12, 281–296. [PubMed: 26584231]

(95). Jacobson MP; Pincus DL; Rapp CS; Day TJ; Honig B; Shaw DE; Friesner RA A Hierarchical Approach to All-Atom Protein Loop Prediction. Proteins: Struct., Funct., Genet 2004, 55, 351–367. [PubMed: 15048827]

(96). Schrödinger Release 2018–1: LigPrep; Schrödinger, LLC, New York, NY, 2018.

(97). Schrödinger Release 2018–1: Prime; Schrödinger, LLC, New York, NY, 2018.

(98). Friesner RA; Banks JL; Murphy RB; Halgren TA; Klicic JJ; Mainz DT; Repasky MP; Knoll EH; Shelley M; Perry JK; Shaw DE; Francis P; Shenkin PS Glide: A New Approach for Rapid, Accurate Docking and Scoring. 1. Method and Assessment of Docking Accuracy. J. Med. Chem 2004, 47, 1739–1749. [PubMed: 15027865]

(99). Dhanachandra Singh K; Karthikeyan M; Kirubakaran P; Nagamani S Pharmacophore Filtering and 3D-QSAR in the Discovery of New JAK2 inhibitors. J. Mol. Graphics Modell 2011, 30, 186–197.

(100). Osajima T; Suzuki M; Neya S; Hoshino T Computational and Statistical Study on the Molecular Interaction between Antigen and Antibody. J. Mol. Graphics Modell 2014, 53, 128–139.

(101). Sun H; Tian S; Zhou S; Li Y; Li D; Xu L; Shen M; Pan P; Hou T Revealing the Favorable Dissociation Pathway of Type II Kinase Inhibitors via Enhanced Sampling Simulations and Two-End-State Calculations. Sci. Rep 2015, 5, 8457. [PubMed: 25678308]

(102). Zhang X; Perez-Sanchez H; Lightstone FC A Comprehensive Docking and MM/GBSA Rescoring Study of Ligand Recognition upon Binding Antithrombin. Curr. Top. Med. Chem 2017, 17, 1631–1639. [PubMed: 27852201]

(103). Braganza LF; Worcester DL Hydrostatic Pressure Induces Hydrocarbon Chain Inter digitation in Single-Component Phospholipid Bilayers. Biochemistry 1986, 25, 2591–2596. [PubMed: 3718966]

(104). Nath Chakraborty SN; Gelb LD A Monte Carlo Simulation Study of Methane Clathrate Hydrates Confined in Slit-Shaped Pores. J. Phys. Chem. B 2012, 116, 2183–2197. [PubMed: 22320214]

(105). Faraldo-Gomez JD; Smith GR; Sansom MS Setting Up and Optimization of Membrane Protein Simulations. Eur. Biophys. J 2002, 31, 217–227. [PubMed: 12029334]

Author Manuscript Author Manuscript Author Manuscript Author Manuscript

(106). Schlegel B; Sippl W; Holtje HD Molecular Dynamics Simulations of Bovine Rhodopsin: Influence of Protonation States and Different Membrane-Mimicking Environments. J. Mol. Model 2005, 12, 49–64. [PubMed: 16247601]

(107). Darden T; York D; Pedersen L Particle Mesh Ewald: an N log (N) Method for Ewald Sums in Large Systems. J. Chem. Phys 1993, 98, 10089–10092.

(108). Isberg V; Balle T; Sander T; Jorgensen FS; Gloriam DE G Protein- and Agonist-Bound Serotonin 5-HT2A Receptor Model Activated by Steered Molecular Dynamics Simulations. J. Chem. Inf. Model 2011, 51, 315–325. [PubMed: 21261291]

Author Manuscript Author Manuscript Author Manuscript Author Manuscript

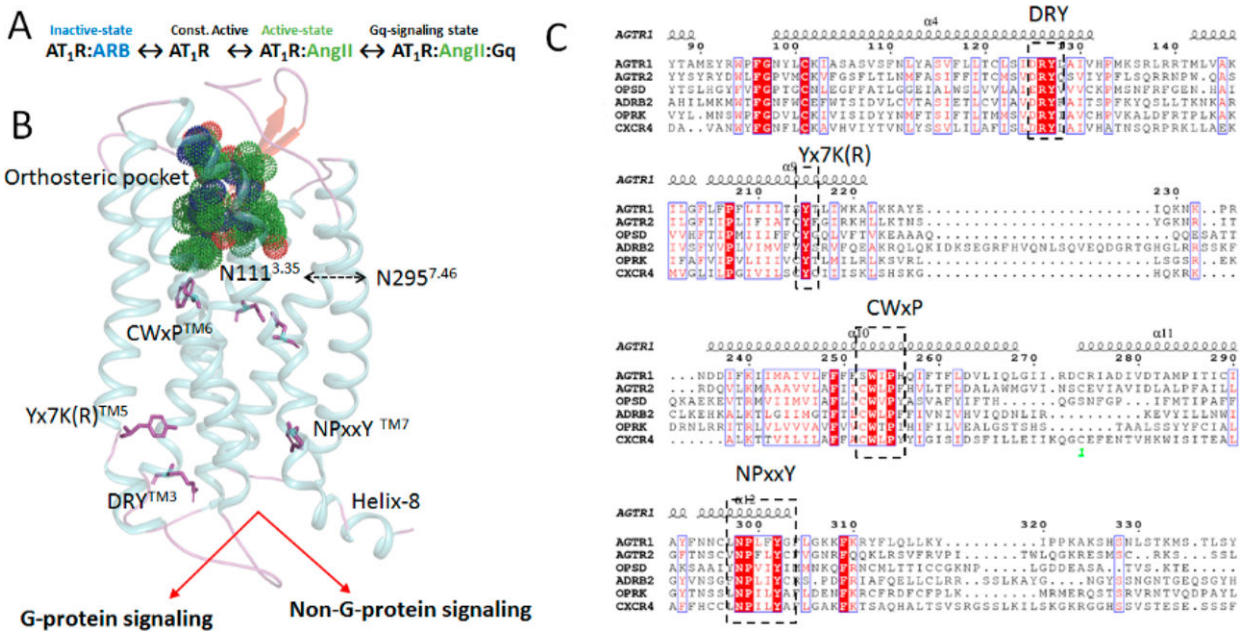

Figure 1.

(A) Scheme of proposed conformational states governing AT_1R function. (B) 3D structure of AT_1R showing orthosteric pocket and important motifs in G-protein and non-G-protein signaling. (C) Multiple sequence alignment of AT_1R with Class A GPCRs highlighting conserved motifs.

Author Manuscript Author Manuscript Author Manuscript Author Manuscript

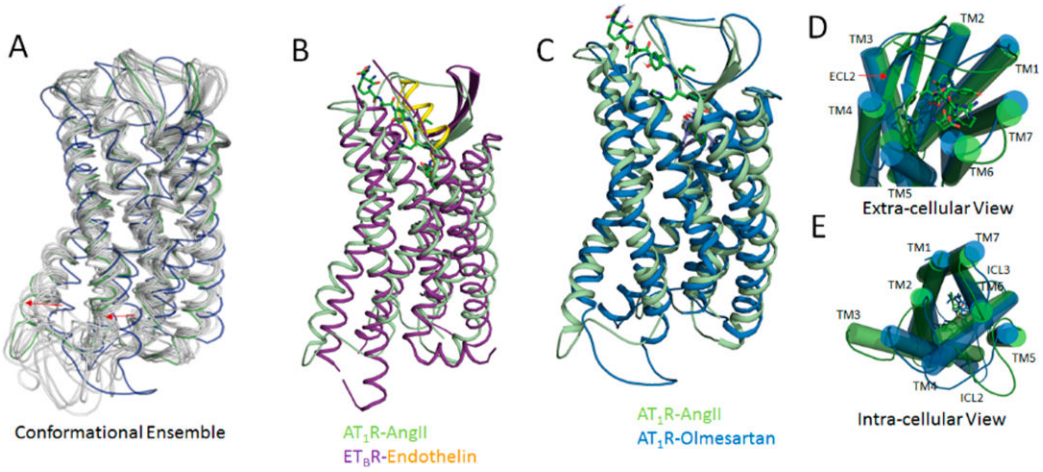

Figure 2.

(A) Representative conformational ensembles from 1 μs MDS of AngII bound AT_1R. (B) Superimposed structure of AT_1R-AngII and ET_BR-Endothelin. Superimposed structure of AT_1R-AngII (from MDS) and AT_1R-Olmesartan (crystal structure) bound states showing transmembrane view (C), extra-cellular view (D), and intra-cellular view (E).

Author Manuscript Author Manuscript Author Manuscript Author Manuscript

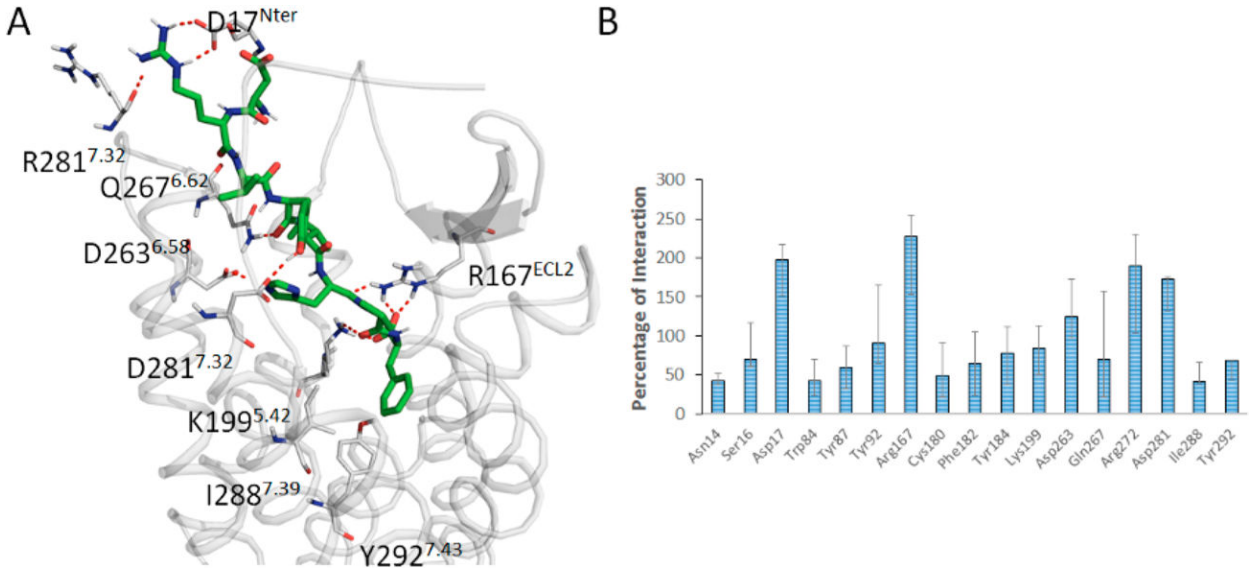

Figure 3.

(A) Binding mode of AngII in the orthosteric pocket of AT_1R. (B) Interaction of AngII with AT_1R residues >25% in at least 3 out of 6 independent MDS experiments are shown. A single residue can have >100% value due to multiple interactions (e.g., weak, ionic, hydrophobic, etc.).

Author Manuscript Author Manuscript Author Manuscript Author Manuscript

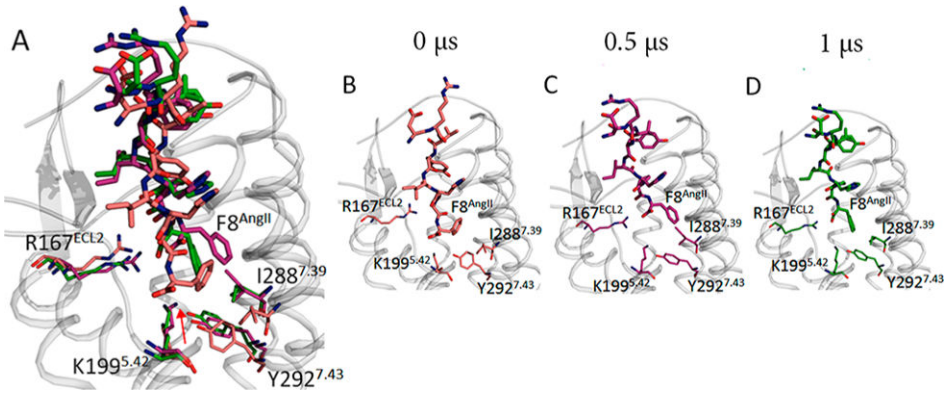

Figure 4.

(A) Superimposed Phe8^{AngII} orientation changes at time intervals indicated. Orientation of Phe8^{AngII} captured at 0 (B), 0.5 (C), and 1 μs (D).

Author Manuscript Author Manuscript Author Manuscript Author Manuscript

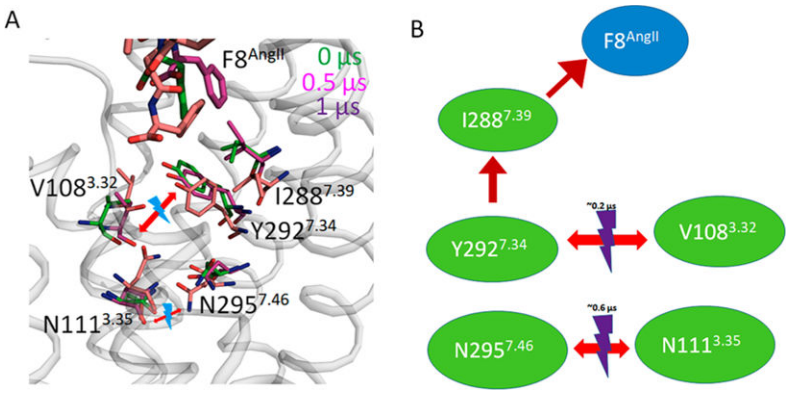

Figure 5.

Representation of Phe8^{AngII} induced motion of side chains leading to breakage of N111$^{3.35}$-N295$^{7.46}$ H-bond.

Author Manuscript Author Manuscript Author Manuscript Author Manuscript

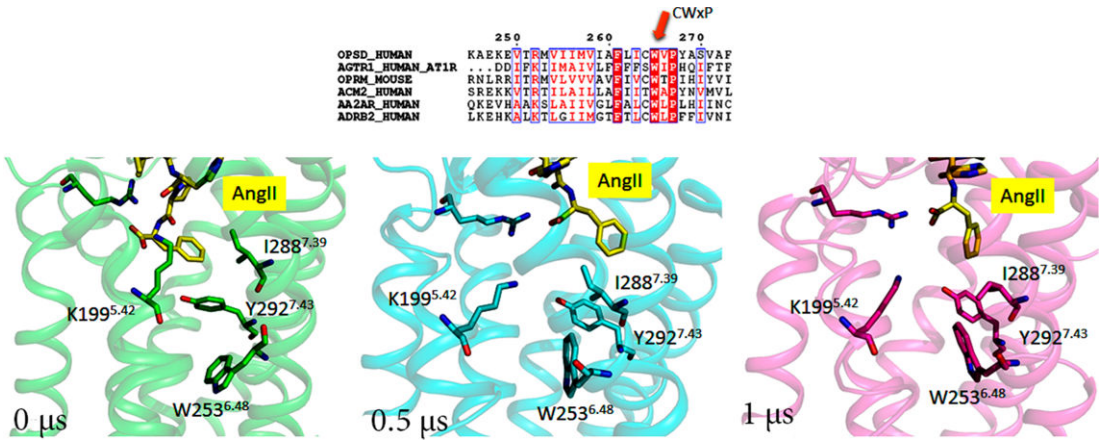

Figure 6.

Conformation of toggle switch $Trp253^{6.48}$ of AT_1R at different time intervals.

Author Manuscript Author Manuscript Author Manuscript Author Manuscript

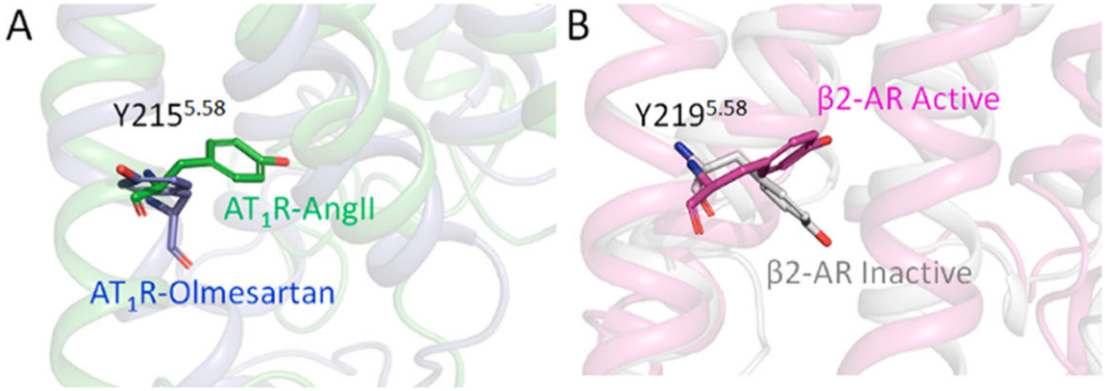

Figure 7.

Conformation of Tyr215$^{5.58}$ projecting inward in AngII-bound AT_1R and outward in olmesartan-bound AT_1R (A). The same pattern is also observed in active and inactive states of β_2AR (B).

Author Manuscript Author Manuscript Author Manuscript Author Manuscript

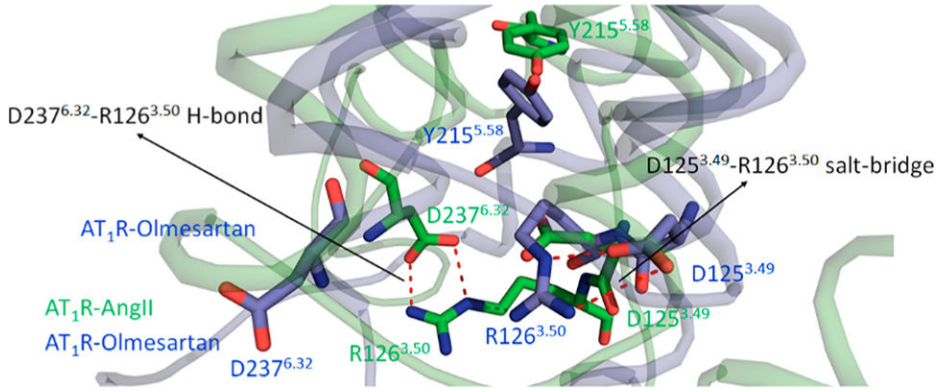

Figure 8.

Breakage of H-bond between D125$^{3.49}$-R126$^{3.50}$ and formation of H-bond between R126$^{3.50}$-D237$^{6.32}$ in AngII bound AT$_1$R. The D125$^{3.49}$-R126$^{3.50}$ H-bond is retained in the olmesartan-bound state.

Author Manuscript Author Manuscript Author Manuscript Author Manuscript

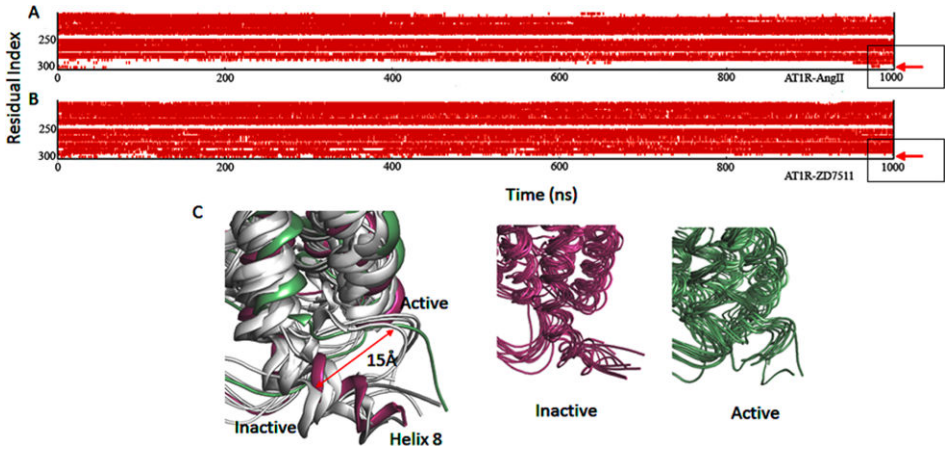

Figure 9.

Secondary structure of H8 region of AT_1R-AngII (A) and AT_1R-ZD7511 (B). Loss of α helix (red color) from residue number 302 to 316 in panel A. Ensembles of structures of AT_1R-AngII and AT_1R-ZD7511 (C).

Author Manuscript

Author Manuscript

Author Manuscript

Author Manuscript

Table 1.

Time Course of Molecular Events Observed in MD Simulation[a]

	Molecular Events	
time	**AT_1R-AngII**	**AT_1R-olmesartan**
0 ns	strong interaction of $Phe8^{AngII}$-$Ile288^{7.39}$	strong interaction of alkyl tail of omesartan-$Ile288^{7.39}$
~200 ns	$Phe8^{AngII}$ pulls up $Ile288^{7.39}$	position of $Ile288^{7.39}$ remain same, strong interaction with alkyl tail of Omesartan
~400 ns	breakage of $Val108^{3.35}$ Cα-OH-$Tyr292^{7.34}$ H-bond (TM3-TM7)	$Val108^{3.32}$ Cα-OH-$Tyr292^{7.34}$ (TM3-TM7) H-bond is consistent
~600 ns	breakage of $Asn111^{3.32}$ $N295^{7.46}$ H-bond (TM3-TM7)	$Asn111^{3.32}$ $N295^{7.46}$ H-bond (TM3-TM7) is consistent
~700	opening of intracellular domain for Gprotein binding	intracellular domain are closed for Gprotein binding
~1000 ns	open intracellular domain with active like conformation	closed intracellular domain with inactive conformation

[a]All these events are captured and shown in MDS trajectory videos1−4.